JOURNAL OF SOLID STATE CHEMISTRY 105, 417–427 (1993)

Crystal Structure and Magnetic Study of a New Iron (III) Phosphate, $Fe_{1.21}PO_4X$ (X = F, OH, H_2O), Isostructural with $3MgSO_4$, $Mg(OH)_2$, H_2O

TH. LOISEAU,* PH. LACORRE,* Y. CALAGE,*,† J. M. GRENÈCHE,† AND G. FÉREY*

Laboratoire des Fluorures, URA C.N.R.S. 449, and †Equipe de Physique de l'Etat Condensé, URA C.N.R.S. 807, Faculté des Sciences, Université du Maine, Avenue Olivier Messiaen, 72017 Le Mans cedex, France

Received November 6, 1992; accepted January 5, 1993

$Fe^{3+}_{1.21}PO_4X$ ($X = F^-$, OH^-, H_2O), obtained by hydrothermal synthesis (200°C, 6 days) from a 1 : 1 : 2 : 40 mixture of $Fe(NO_3)_3(H_2O)_9$, P_2O_5, NH_4F, H_2O, is tetragonal (S.G. = $I4_1/amd$ (No. 141)), a = 5.184(1) Å, c = 13.040(5) Å, V = 350.4(3) Å^3, Z = 4. Its structure, isotypic with those of Lipscombite, $Fe_{2-\delta}PO_4(OH)$, and $3MgSO_4$, $Mg(OH)_2$, H_2O, is built up from the interconnection of chains of face sharing anionic octahedra (5 × 14 Å^2 structure type). The partial occupancy, close to $\frac{2}{3}$, of these octahedra by Fe^{3+} is discussed. Antiferromagnetism (T_N = 81 K) of $Fe_{1.21}PO_4X$ was characterized by susceptibility measurements and Mössbauer spectroscopy. The magnetic behavior is analyzed in relation with the two types of disorder (vacancies and nature of X) occuring in the chains.

Introduction

Since 1982 and the discovery of AlPO microporous compounds (*1*), much attention has been paid to the systems M_2O_3–P_2O_5–H_2O–amine (M = Al, Ga) (see for instance (*2*, *3*)). More recently, Kessler (*4*) studied some of these systems in fluorinated media and showed that fluoride ions, primitively thought to act as mineralizers, in fact participate in the reaction and are incorporated into the framework of the microporous compound.

In order to understand the respective roles of the amine and of F^- in the synthesis of microporous compounds, we have undertaken a general survey of the hydrothermal behavior of the systems M_2O_3–P_2O_5–NH_4F and/or amine–H_2O (M = Al, Ga, Fe, V). This paper deals with the phase $Fe_{1.21}PO_4X$ (X = F, OH, H_2O), which occurs in the system Fe_2O_3–P_2O_5–NH_4F–H_2O. We present here its crystal structure, strongly related to those of Lipscombite, $Fe_{2-\delta}PO_4(OH)$ (*5*, *6*), and $3MgSO_4$, $Mg(OH)_2$, H_2O (*7*), and its magnetic properties, studied by susceptibility measurements and Mössbauer spectroscopy.

Experimental

Synthesis and Characterization

The synthesis was carried out hydrothermally from a mixture corresponding to the molecular ratio 1 $Fe(NO_3)_3$,$9H_2O$; 1 P_2O_5; 2 NH_4F; 40 H_2O. These compounds were placed in a stainless steel autoclave lined with Teflon and heated at 200°C for 6 days. The resulting product was a pale brown powder which was filtered off, washed with distilled water, and dried at room temperature. The X-ray powder pattern exhibits strong similarities to that of $3MgSO_4$, $Mg(OH)_2$, H_2O (*7*), hereafter denoted MHSH.

The fluorine content was determined by

0022-4596/93 $5.00

the potentiometric method with a fluorine-specific electrode.

Crystal Structure Determination

A pale brown elongated octahedral single crystal was selected by optical examination for structure determination. Intensity data were collected on a Siemens AED-2 four-circle diffractometer with conditions of data measurement reported in Table I. The cell parameters were obtained from a long exposure rotation photograph and refined from 36 reflections measured in double step scan at $\pm 2\theta \approx 30°$. The $4/mmm$ point symmetry was confirmed from intensity measurement of two $4/mmm$ independent sets corresponding to one $4/m$ independent set. The averaging of intensities in $4/mmm$ led to $R = 0.014$. The scattering factors and anomalous dispersion corrections for all atoms are taken from the International Tables for X-Ray Crystallography. Absorption corrections were applied using the Gaussian method. The structure was refined with the SHELX-76 program system (8), in the $I4_1/amd$ space group, deduced from the observed systematic intensity extinctions.

Mössbauer Spectroscopy

Mössbauer experiments were performed over the temperature range 2–300 K, using a constant acceleration signal spectrometer with a ^{57}Co source diffused into a rhodium matrix. The sample, resulting from a mixture of powdered $Fe_{1.21}PO_4X$ and boron nitride with 5 mg iron per cm^2, was located in a bath cryostat with a standard regulator whose accuracy is estimated at 0.1 K. The Mössbauer spectra were fitted using the MOSFIT program (9).

Magnetic Susceptibility

Between 4.2 and 300 K, the magnetic susceptibility was measured by the Faraday method. The powder sample was cooled both with and without applied magnetic field.

TABLE I

CONDITIONS OF X-RAY DATA COLLECTION FROM $Fe_{1.21}PO_4F_{0.45}(OH)_{0.18}(H_2O)_{0.37}$

Determination of cell parameters	36 reflections at $\pm 2\theta \approx 30°$
Space group	$I4_1/amd$ (No. 141)
Cell dimensions	$a = 5.184(1)$ Å $c = 13.040(5)$ Å
Volume/Z	350.4(3) Å^3/$Z = 4$
Wavelength/monochromator	0.71069 Å (Mo$K\alpha$)/graphite
Temperature	293 K
Scan mode	ω-2θ
Step scan	$39 \leq N \leq 45$, every 0.035° and 4 sec
Aperture	3.5 × 3.5 mm^2
Crystal dimensions	0.08 × 0.08 × 0.10 mm^3
Crystal faces	±(101, 10 −1, 011, 01 −1)
Absorption corrections	Gaussian method
Transmission factors	$T_{min} = 0.586$; $T_{max} = 0.700$
Absorption coefficient	$\mu = 66.3$ cm^{-1}
Angular range of data collection	$2\theta \leq 70°$
Range of measured h, k, l	$0 \leq h \leq 8$; $0 \leq k \leq 8$; $0 \leq l \leq 20$
Standard reflections (3)	4 0 0; 0 4 0; −2 −1 3
Measured every	60 min
Maximum intensity variation	4.4%
Measured reflections	404
Independent Ref. ($\|F\| > 6\sigma(\|F\|)$)	165
Weight	$w = 1.024/(\sigma^2(F) + 0.000085F^2)$
Secondary extinction	$X = 4.8 \times 10^{-7}$
Number of refined parameters	19
Final Fourier residuals	−0.25 to +0.46 e Å^{-3}
R/R_w	0.020/0.021

Structure Refinement and Discussion

Owing to the great similarities between the X-ray powder diffraction pattern of the iron phosphate and that of $3MgSO_4$, $Mg(OH)_2$, H_2O (7), the structure was determined by starting from the coordinates of the latter with iron replacing magnesium and phosphorus replacing sulfur; hydrogen

atoms were omitted in a first step. The reliability factor converged to $R = 0.170$. At this step of the refinement, a large isotropic thermal parameter on the iron sites (8d) was observed. The local symmetry of each iron site was lowered, allowing random distribution of iron atoms over two symmetry-equivalent sites (16h), as suggested in Ref. (*7*); the reliability factor then fell to $R = 0.080$. The refinement of the occupancy factor of iron (0.302 instead of 0.333 for Mg in MHSH and from 0.375 to 0.438 in Lipscombite) and of the anisotropic thermal parameters led to $R = 0.026$. The low thermal parameters of the oxygen (4b) suggested the possibility of partial substitution by fluorine. Chemical analysis gave 0.45(5) F^- per PO_4 unit. In the structure refinement, when oxygen is replaced by fluorine on this site, the reliability factor is lowered to $R = 0.023$. However, the existence of residues (electronic density of 0.46 e Å^{-3}) near the 4b site (0.87 Å) could be assigned to hydrogen atoms, and would correspond to a hydroxyl group or water molecule as in MHSH. However, hydrogen atoms were not positioned because of the weak electronic density of the residues. A final refinement of F^-/O^{2-} on the 4b site led to reliability factors $R = 0.020$ and $R_w = 0.021$, with 45% F^- and 55% O^{2-}, in agreement with the chemical analysis.

As no divalent iron was evidenced by the Mössbauer study (see the following section), the amount of water in the formula was deduced from electroneutrality calculations assuming previous statistical occupancy of the 4b site. Thus, the formula of the compound has been stated as

$$Fe_{1+x}PO_4[F_y(OH_{3x-y}(H_2O)_{1-3x}]$$
$$\text{with } x = 0.21(1) \quad \text{and} \quad y = 0.45(5),$$

the 4b site being statistically occupied by F^-, OH^- and H_2O (in brackets in the formula).

The atomic coordinates and anisotropic thermal parameters are reported in Tables II and III, respectively. Selected interatomic distances and bond angles are listed in Table IV.

The compound is isostructural with $3MgSO_4$, $Mg(OH)_2$, H_2O, belonging to the 5×14 Å^2 type structures (*10*). The structure is built up from $Fe_2O_4X_2$ (X = F^-, OH^- or H_2O) octahedra and PO_4 tetrahedra. The face-sharing octahedra form infinite straight chains along [100] at $z = \frac{1}{4}$ and $z = \frac{3}{4}$ and along [010] at $z = 0$ and $z = \frac{1}{2}$. Two chains at different levels are interconnected via both X molecules and PO_4 tetrahedra (Fig. 1). This is another example of the O'Keeffe–Andersson rod packing structures (*11*).

Most interesting is what happens in the chains, and the magnetic consequences of this situation.

In the structural type, the chains can accommodate various amounts of vacancies (from 11% in Lipscombite to 33% in MHSH and 40% in our case). In MHSH, the magnesium atoms occupy exactly two thirds of the face-sharing octahedra of a chain (*7*). As claimed by the authors, it is reasonable to think that, within a chain, there exists a strict ordering between cations and vacancies, in the same way as in the 2H hexagonal perovskite $Cs_3\square Fe_2F_9$ (*12*) built up from a similar type of chains. But in MHSH, the connection between two chains via X can lead to three different, energetically degenerated, situations around X ((i) 4 filled octahedra, (ii) 3 filled and 1 empty, (iii) 2 filled and 2 empty) which explain the apparent disorder from one ordered chain to the other, leading to the mean space group $I4_1/amd$. A similar situation has previously been encountered in $BaCuFeF_7$ (*13*), for instance.

In $Fe_{1.21}PO_4X$, the splitting of iron atoms between two 16h positions inside octahedra suggests that the most common situation is that of bioctahedral units: the splitting reflects the electrostatic repulsion between adjacent Fe^{3+}. It results in a maximum spread in Fe–O and Fe–X distances of about ±7.2% relative to the mean distance (from 1.91 Å to 2.21 Å, see Table IV), slightly

TABLE II

ATOMIC COORDINATES AND MEAN-SQUARE DISPLACEMENTS FOR $Fe_{1.21}PO_4F_{0.45}(OH)_{0.18}(H_2O)_{0.37}$

Atom	Occupancy	Site	X	Y	Z	B_{eq}
Fe	0.303(1)	16h	0	0.0330(6)	0.4988(4)	0.90(7)
P	1	4a	0	$\frac{3}{4}$	$\frac{1}{8}$	0.86(3)
O	1	16h	0	0.5058(4)	0.1912(1)	2.22(8)
X^a	1	4b	0	$\frac{1}{4}$	$\frac{3}{8}$	1.48(5)

Note. B_{eq} (Å^2) is defined as $B_{eq} = 8\pi^2(U_{11} + U_{22} + U_{33})/3$

[a] $X = 0.45(5)\ F^- + 0.55(5)\ O^{2-}$.

TABLE III

ANISOTROPIC THERMAL PARAMETERS[a] FOR $Fe_{1.21}PO_4F_{0.45}(OH)_{0.18}(H_2O)_{0.37}$ ($U_{ij} \times 10^4$ Å^2)

Atom	U_{11}	U_{22}	U_{33}	U_{23}	U_{13}	U_{12}
Fe	107(4)	112(18)	122(4)	−2(10)	0	0
P	104(4)	104(4)	118(4)	0	0	0
O	247(10)	273(11)	322(10)	172(10)	0	0
X^b	197(11)	197(11)	168(13)	0	0	0

[a] The vibrational coefficients relate to the expression $T = \exp[-2\pi^2(h^2a^{*2}U_{11} + k^2b^{*2}U_{22} + l^2c^{*2}U_{33} + 2klb^*c^*U_{23} + 2hla^*c^*U_{13} + 2hka^*b^*U_{12})]$.

[b] $X = 0.45(5)\ F^- + 0.55(5)\ O^{2-}$.

TABLE IV

INTERATOMIC DISTANCES (Å) AND ANGLES (°) IN $Fe_{1.21}PO_4F_{0.45}(OH)_{0.18}(H_2O)_{0.37}$

P–O	1.532(4)	(4×)	$O_{(V,VII)}$–P–$O_{(VI,VIII)}$	108.5(3)	(4×)
			$O_{(V)}$–P–$O_{(VIII)}$	111.4(2)	(1×)
			$O_{(VI)}$–P–$O_{(VII)}$	111.4(3)	(1×)
Fe–$O_{(I,II)}$	1.907(3)	(2×)	$O_{(i)}$–Fe–$O_{(II)}$	88.1(2)	(1×)
Fe–$O_{(III,IV)}$	2.115(3)	(2×)	$O_{(I,II)}$–Fe–$O_{(III)}$	172.2(2)	(2×)
Fe–$X_{(i)}$	1.968(5)	(1×)	$O_{(I,II)}$–Fe–$O_{(IV)}$	96.8(2)	(2×)
Fe–$X_{(ii)}$	2.205(4)	(1×)	$O_{(I,II)}$–Fe–$X_{(i)}$	90.0(3)	(2×)
			$O_{(I,II)}$–Fe–$X_{(ii)}$	95.0(2)	(2×)
			$O_{(III)}$–Fe–$O_{(IV)}$	77.6(2)	(1×)
			$O_{(III,IV)}$–Fe–$X_{(ii)}$	78.7(3)	(2×)
			$X_{(i)}$–Fe–$X_{(ii)}$	173.2(1)	(1×)
			$X_{(i)}$–Fe–$O_{(III,IV)}$	96.0(2)	(2×)

$X = F^-$ or O^{2-}

Symmetry codes

(I)	$\frac{3}{4} + y$	$\frac{1}{4}$	$\frac{3}{4} - z$	(V)	0	$\frac{1}{2} - y$	z
(II)	$\frac{1}{4} - y$	$\frac{1}{4}$	$\frac{3}{4} - z$	(VI)	$\frac{1}{4} + y$	$\frac{3}{4}$	$-z$
(III)	$\frac{1}{4} - y$	$\frac{3}{4}$	$\frac{1}{4} + z$	(VII)	$\frac{3}{4} - y$	$\frac{3}{4}$	$\frac{1}{4} - z$
(IV)	$\frac{3}{4} + y$	$\frac{3}{4}$	$\frac{1}{4} + z$	(VIII)	x	y	z
(i)	0	$\frac{1}{4}$	$\frac{3}{8}$	(ii)	0	$\frac{3}{4}$	$\frac{5}{8}$

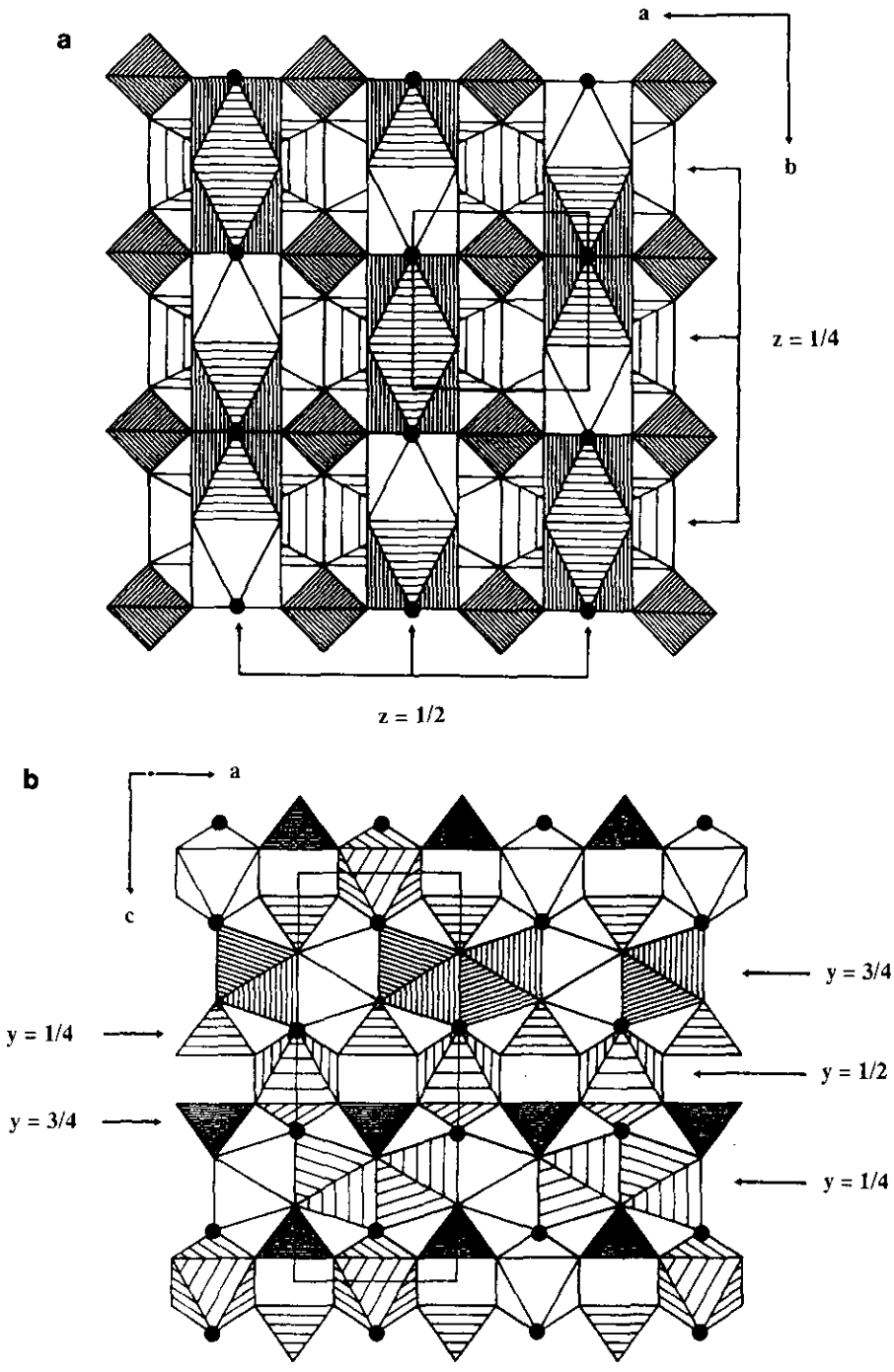

FIG. 1. Local polyhedral arrangement of $Fe_{1.21}PO_4X$. An ideal vacancies ordering (2 filled sites/1 vacant site) has been represented within each octahedral chain, with no coherence between chains (hatched octahedra occupied by iron atoms). The macroscopic structure as determined from X-ray diffraction show a statistical occupancy (60%) of octahedral sites. Black circles represent the special position 4b occupied by the atom X ($X = F^-$ or O^{2-}). (a) Projection along c ($0 < z \leq \frac{1}{2}$). (b) Projection along b ($0 \leq z < 1$).

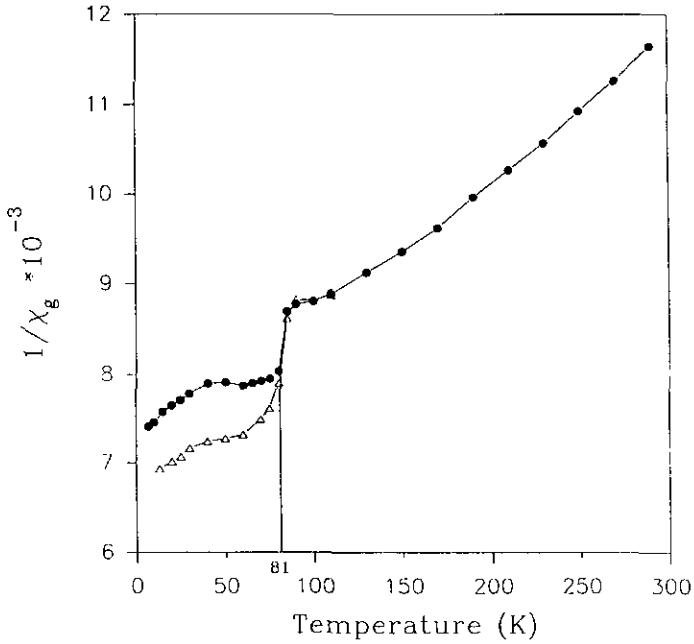

FIG. 2. Thermal evolution of the inverse magnetic susceptibility versus the temperature (Δ cooling with magnetic field; ● cooling without magnetic field).

wider than that (±5.6%) observed in $Cs_3\square Fe_2F_9$ (from 1.84 Å to 2.06 Å, see Ref. (*12*)). In the latter compound, however, only one sort of anion is present. In addition, in $Fe_{1.21}PO_4X$, the local intrachain order is less strict, since less than $\frac{2}{3}$ of the octahedra are occupied. This means that within a chain the 1 : 2 vacancy-cation order is not strict: on a sufficiently long distance, some isolated Fe^{3+} octahedra and/or two adjacent empty octahedra can be encountered. The diversity of the local situations, and the correlative variety of possibilities concerning the chemical nature of X (F^-, OH^-, H_2O) must have drastic consequences on the magnetic behavior which should reflect the cation-vacancy disorder and the existence of different superexchange integrals due to the nature of X. A study was undertaken using both magnetic susceptibility measurements and Mössbauer spectroscopy.

Magnetic Behavior and Discussion

The thermal variation of the inverse susceptibility (Fig. 2) is typical of a canted antiferromagnet (T_N = 81 K). The difference between the measurements for a sample cooled with and without applied magnetic field indicates some fluctuations of the spins.

The Mössbauer spectra, recorded at 90 K and 300 K (see Fig. 3), reveal that the hyperfine structure results only from the presence of pure electric interactions. These two paramagnetic spectra exhibit two broadened and overlapped lines with a weak asymmetry. Both were well reproduced by considering at least two quadrupolar components. The refined values of the hyperfine parameters are reported in Table V: the isomer shift values give clear evidence for six-fold coordinated trivalent high-spin iron ions. No divalent iron phase is observed in these spectra.

The most significant magnetic spectra recorded below 83 K are given in Fig. 4. One can distinguish two temperature ranges, according to the nature of the hyperfine structures of Mössbauer spectra:

—Between 65 and 83 K, the hyperfine structure appears rather complex; the spec-

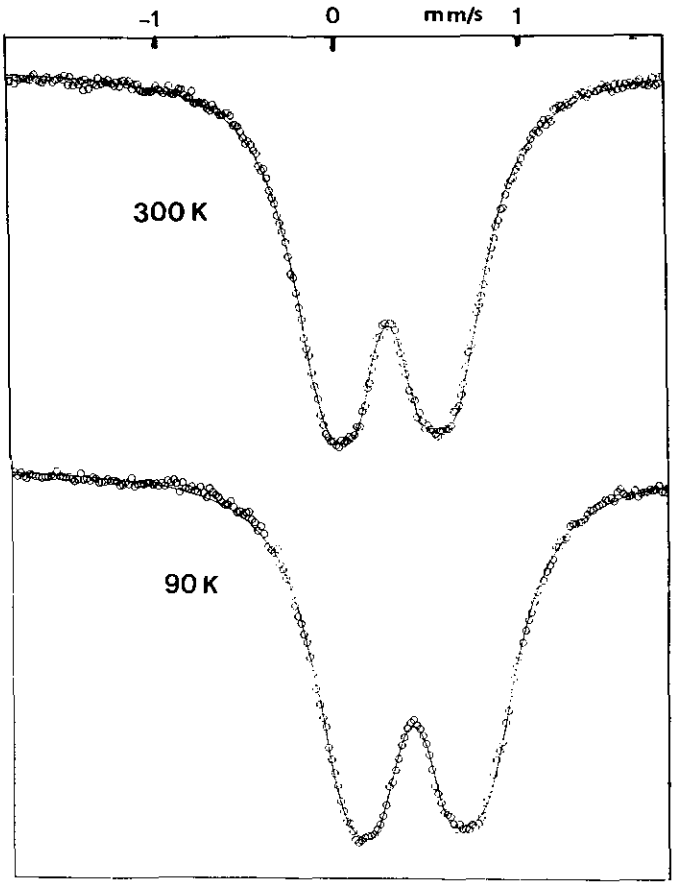

FIG. 3. Mössbauer spectra of $Fe_{1.21}PO_4X$ in the paramagnetic state.

tra are composed of superimposed magnetic and paramagnetic contributions whose respective proportions depend on the temperature. The paramagnetic fraction is reported in Fig. 5. The appearance of a magnetic ordering transition at 83 K is consistent with the accident which occurs on the magnetic susceptibility curve around the same temperature.

—At temperatures lower than 65 K, the Mössbauer spectra result from magnetic sextets with broad lines, except at the lower temperatures, and with an asymmetric hyperfine structure. The presence of broad and asymmetric lines is significant of a structural disorder and probably reflects the different cationic and anionic neighboring of iron nuclei, as expected. However, the presence of well defined lines at 4.2 K allows us to conclude that at least two main magnetic contributions have been superposed.

By looking at the evolution of the spectra recorded at 4.2, 30, and 55 K, one can obtain information relative to the shape of both hyperfine field distributions. In fact, the intensity of the outer sextet decreases as the temperature increases, while the internal wings of the outer "line doublets" become more important as the temperature increases: it can be concluded that (i) the distribution of hyperfine fields associated with the higher values is very sharp at low temperature and evolves strongly with the occurrence of a low field tail as the temperature increases, and (ii) the shape of the second distribution is less sensitive to the temperature.

TABLE V

HYPERFINE CHARACTERISTICS OF $Fe_{1.2}PO_4X$ (X = F, OH, H_2O)

	Paramagnetic phases				Magnetic phases				
T (K)	P (%)	IS (mm/sec)	QS (mm/sec)	Γ (mm/sec)	M (%)	IS (mm/sec)	2ε (mm/sec)	Γ (mm/sec)	$\langle H_f \rangle$ (kOe)
300	75	0.413	0.714	0.44	0	—	—	—	—
	25	0.401	0.339	0.27					
90	68	0.522	0.771	0.44	0	—	—	—	—
	32	0.512	0.375	0.32	0				
81	27	0.48	0.77	0.36	54	0.48	−0.20	0.40	115
	19	0.48	0.38	0.36					
80	25	0.48	0.77	0.36	54	0.48	−0.20	0.40	134
	15	0.48	0.38	0.36	6	0.48	0.08	0.40	180
77	18	0.49	0.77	0.36	60	0.49	−0.20	0.40	210
	11	0.49	0.38	0.36	11	0.49	0.08	0.40	245
75	12	0.49	0.77	0.36	51	0.49	−0.20	0.40	250
	4	0.49	0.38	0.36	33	0.49	0.08	0.40	261
70	11	0.51	0.77	0.36	58	0.51	−0.20	0.40	305
	2	0.51	0.38	0.36	29	0.51	0.08	0.40	213
67	7	0.50	0.77	0.36	58	0.50	−0.20	0.40	320
	3	0.50	0.38	0.36	32	0.50	0.08	0.40	330
65	3	0.52	0.77	0.36	71	0.52	−0.20	0.40	323
	0				26	0.52	0.08	0.40	339
60	—	—	—	—	78	0.49	−0.20	0.32	365
					22	0.48	0.09	0.32	370
55	—	—	—	—	71	0.51	−0.21	0.43	379
					29	0.50	0.09	0.30	375
30	—	—	—	—	75	0.51	−0.20	0.32	492
					25	0.51	0.09	0.32	474
4.2	—	—	—	—	68	0.52	−0.20	0.45	519
					32	0.52	0.09	0.30	485

Note. Underlined values were held fixed during the fitting procedure. IS: Isomer shift relative to Fe metal at 300 K. During the fit, in the temperature range 65–81 K, identical values of IS were imposed on all the contributions. QS or 2ε: Quadrupole splitting or quadrupole shift. P(%) or M(%): Paramagnetic or magnetic fraction. $\langle H_F \rangle$: Mean hyperfine field deduced from the hyperfine field distributions for each magnetic contribution.

In the temperature range 65–83 K, the broadening of the magnetic lines weakly increases while the paramagnetic doublet appears in the low velocity range.

After this qualitative description, one can assume two hypotheses in fitting the present set of magnetic spectra.

The first one consists in considering two magnetic ordering temperatures, each one attributed to a different contribution. But this hypothesis is not consistent with the experimental results: (i) the asymmetry of magnetic lines for the spectra recorded in the temperature range 65–83 K is not well reproduced, (ii) the values of the hyperfine parameters for these temperatures are not coherent with those obtained at lower temperatures, and (iii) the thermal evolution of the inverse susceptibility does not reveal two well defined magnetic ordering transitions.

The second hypothesis lies in the existence of a continuous distribution of magnetic ordering temperatures, in the range 65–83 K; the variety of the magnetic hyperfine structures evidenced by the broadening of the lines and the simultaneous presence of paramagnetic and magnetic spin states,

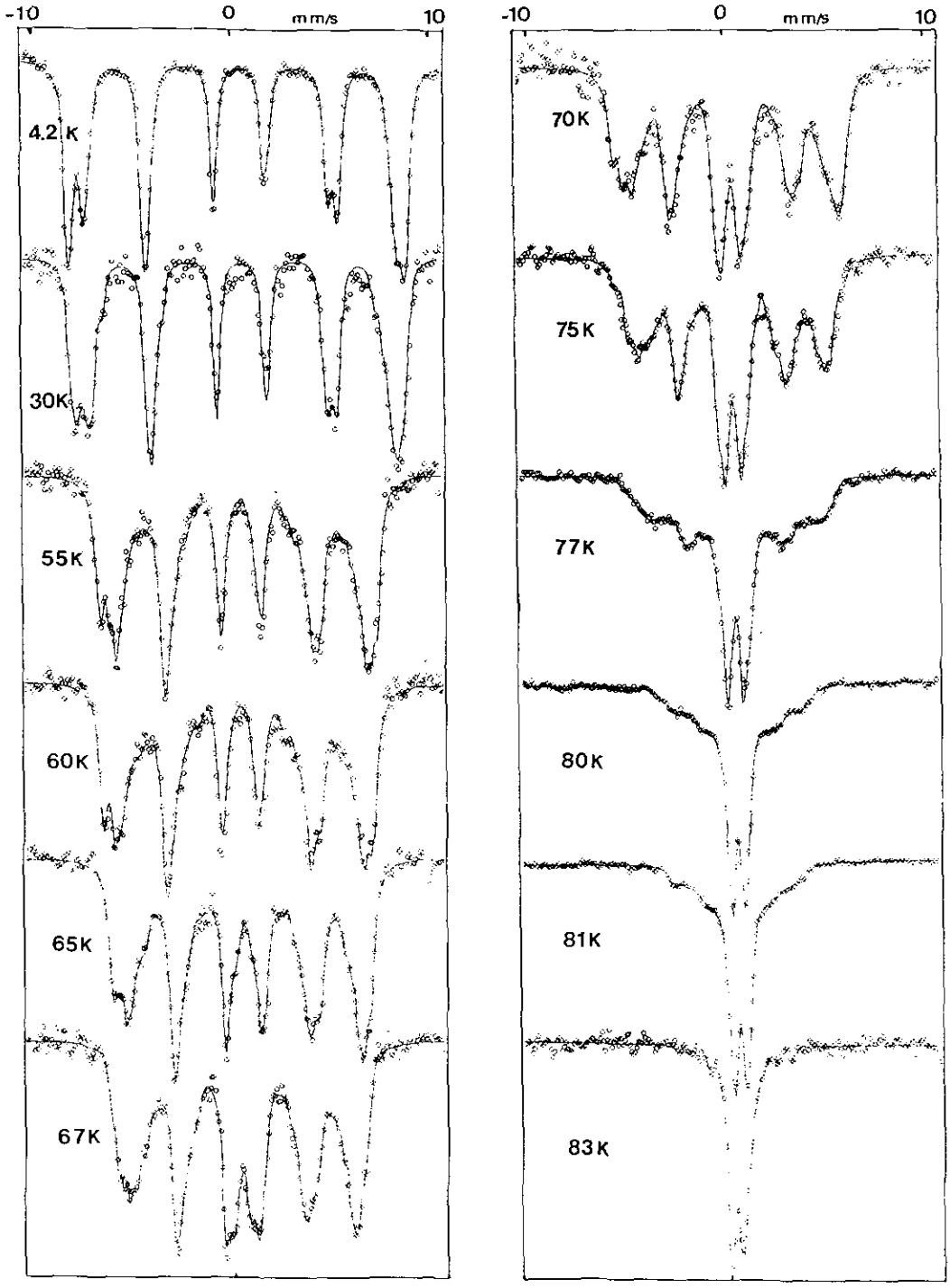

FIG. 4. Thermal evolution of Mössbauer spectra below T_N = 81 K.

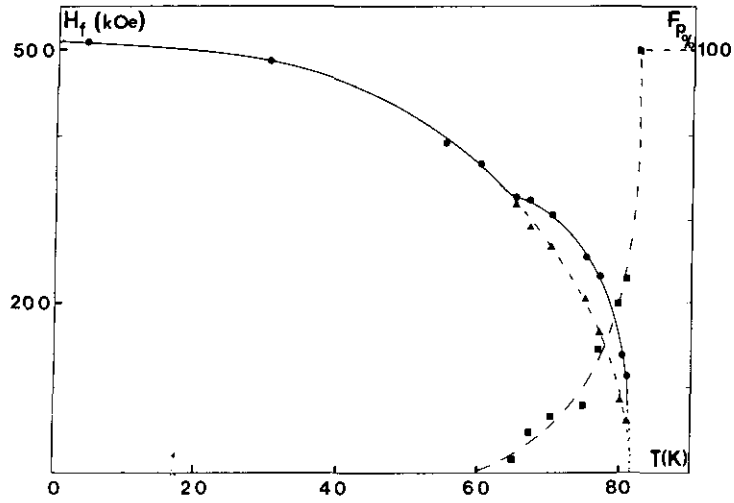

FIG. 5. Thermal evolution of the mean hyperfine field values $\langle H_f \rangle$. (●, ▲ calculations performed with, without accounting for the paramagnetic contribution, respectively) and of the paramagnetic fraction F_p (■).

is assigned to the different topological situations induced by the anionic and cationic disorders. We have considered in the present study two magnetic components with (i) two independent and discrete hyperfine field distributions, (ii) a lorentzian linewidth value fixed at 0.40 mm.s^{-1} for each component, and (iii) quadrupole shift and isomer shift values refined for each component equal, below 65 K. In the range 65–83 K, two additional paramagnetic contributions were accounted for.

The agreement between experimental and theoretical spectra at different temperatures, using this hypothesis, is better than that observed in the first case. The hyperfine data are reported in Table V: one can note a reasonable agreement on the isomer shift values and on the proportions over both magnetic and paramagnetic ranges. The thermal evolution of the mean hyperfine field values, calculated accounting for the paramagnetic contribution or not, confirms the distribution of magnetic ordering temperatures as shown in Fig. 5.

This series of spectra can also be fitted with three independent magnetic components: this hypothesis agrees well with the structural data (see first section), which reveals the existence of three main types of cationic neighboring for Fe^{3+} sites. This fitting procedure, which appears more realistic, is much more difficult to apply to all these spectra, because of the large broadening of the lines: the overlapping range of the hyperfine field distributions leads to an arbitrary choice of (unphysical) constraints in generating these distributions. In addition, the proportions of the components cannot be successfully correlated to those computed from a simple statistical model of tridimensional random packing of strictly ordered chains (see Fig. 1).

The statistical analysis taking into account the distribution of anions and cationic vacancies around iron sites appears to be rather complex and prevents to the establishment of a clear relationship between crystallographic and Mössbauer data. The distribution of magnetic ordering temperatures and the low temperature evolution of the magnetic susceptibility (with the presence of a very broad peak) might be attributed to a magnetic clustering phenomenon: this behavior could originate from the cationic structure with the non-stoichiometry

and the presence of different exchange mechanism (let us mention the nonnegligible role of the supersuperexchange contribution through PO_4 units). This point suggests some further developments.

Acknowledgments

The authors are grateful to Professor Leblanc (Université du Maine) for his help with X-ray data collection.

References

1. S. T. Wilson, B. M. Lok, C. A. Messina, T. R. Cannan, and E. M. Flanigen, *J. Am. Chem. Soc.* **104,** 1146 (1982).
2. J. M. Bennett, W. J. Dytrich, J. J. Pluth, J. W. Richardson, Jr., and J. V. Smith, *Zeolites* **6,** 349 (1986).
3. R. Xu, J. Chen, and S. Feng, *in* "Chemistry of Microporous Crystals," Proceedings of the International Symposium on Chemistry of Microporous Crystals, Tokyo, June 26–29, *Stud. Surf. Sci. Cat.* **60,** 63 (1990).
4. H. Kessler, *in* "Recent Advances in Zeolites Science," *Stud. Surf. Sci. Catal.* **52,** 17 (1989).
5. L. Katz and W. N. Lipscomb, *Acta Crystallogr.* **4,** 345 (1951).
6. I. Vencato, E. Mattievich, and Y. P. Mascarenhas, *Am. Mineral.* **74,** 456 (1989).
7. K. D. Keefer, M. F. Hochella, Jr., and B. H. W. S. De Jong, *Acta Crystallogr. Sect. B* **37,** 1003 (1981).
8. G. M. Sheldrick, "SHELX-76, A Program for Crystal Structure Determination," Univ. of Cambridge, England (1976).
9. J. Teillet and F. Varret, unpublished MOSFIT program.
10. P. B. Moore and A. R. Kampf, *Z. Kristallogr.* **201,** 263 (1992).
11. M. O'Keeffe and S. Andersson, *Acta Crystallogr. Sect. A* **33,** 914 (1977).
12. F. Wall, G. Pausewang, and D. Babel, *J. Less-Common Met.* **25,** 257 (1971); S. Kummer, Thesis, Marburg (1986).
13. G. Férey, J. Renaudin, A. De Kozak, and M. Samouël, *Z. Kristallogr.* **189,** 77 (1989).